DNS analysis of a Re = 40,000 swirl burner

By V. Moureau†, P. Domingo†, L. Vervisch† AND D. Veynante‡

A premixed turbulent combustion Direct Numerical Simulation (DNS) database of a swirl burner is analyzed from three angles: estimation of the three-dimensional flame surface from two-dimensional fields; modeling of subgrid source and flux terms entering the balance equation for the reaction progress variable in Large Eddy Simulation (LES); and modeling of the subgrid-scale scalar variance in LES. The 2.6-billion-cell unstructured mesh DNS features a flow Reynolds number of 40,000 and a turbulent Reynolds number of 1,400. The new model proposed for the subgrid-scale scalar variance is also tested performing LES of the same swirl burner.

1. Background and objectives

Premixed combustion modeling is a challenging task due to the broad range of scales that interact in the flame brush. In Direct Numerical Simulations (DNS), all these scales are resolved, including intermediate radical species that require mesh resolutions around 20 µm under atmospheric conditions for hydrocarbon fuels (Hawkes & Chen 2006). In turbulent combustion modes where the flamelet assumption holds, the flame structure may be mapped onto the major species and solving of intermediate radical species is not mandatory for capturing global flame dynamics. DNS may then be performed using tabulated chemistry with coarser mesh resolutions. This methodology was recently applied in a semi-industrial swirl burner operated with a lean mixture of air and methane (Moureau *et al.* 2010), where the Reynolds number at the swirler exit is approximately 40,000. The database featuring a mesh of 2.6 billion tetrahedra was generated with the YALES2 code developed at CORIA. This database is analyzed through filtering and averaging in order to discriminate and validate existing LES combustion models, and to design a new closure for the subgrid-scale (SGS) variance of scalars.

2. Description of the DNS database and flow solver

The chosen configuration is an aeronautical burner investigated experimentally and numerically (Meier *et al.* 2007; Roux *et al.* 2005; Moureau *et al.* 2007; Galpin *et al.* 2008). YALES2 solves the low-Mach Navier-Stokes equations with a projection method for constant and variable density flows. These equations are discretized with a 4th-order central scheme in space and a 4th-order Runge-Kutta-like scheme in time. The Poisson equation arising in the projection steps is solved with a highly efficient deflated conjugate gradient. The mesh management of YALES2 allows very large meshes of billions of cells to be handled. It features mesh and solution pre-partitioning and homogeneous mesh refinement based on a non-degenerescent tessellation algorithm for tetrahedrons (Rivara 1984).

† CORIA, CNRS UMR6614, Université et INSA de Rouen, Saint-Etienne du Rouvray, France
‡ EM2C, CNRS UPR288, Ecole Centrale Paris, France

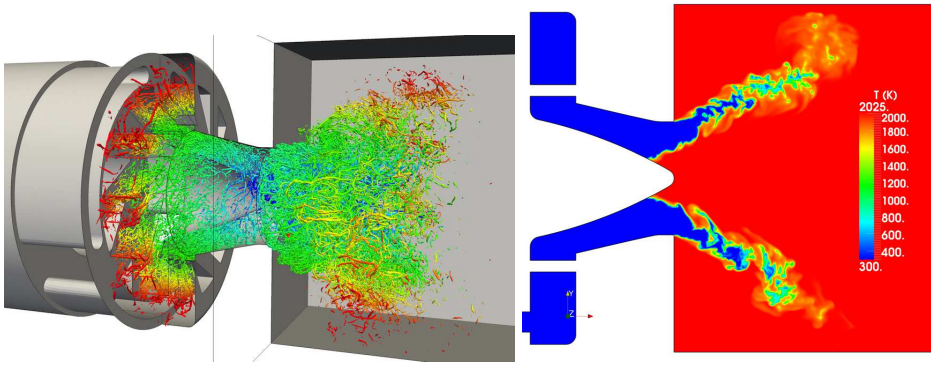

FIGURE 1. Left: Iso-Q criterion in the swirler and in the combustor (cold-flow simulation). Right: Temperature field in the median plane.

In the database, combustion is assumed to be fully premixed, which allows us to model it only through an adequate progress variable. The LES runs are performed with the localized dynamic Smagorinsky model (Germano *et al.* 1991) and the PCM-FPI SGS combustion closure (Domingo *et al.* 2008), whereas the DNS is performed without any model, aside from the premixed flamelet chemistry tabulation.

The DNS features a 2.6-billion-cell unstructured mesh, with a resolution of 100 µm that is sufficient to resolve most of the turbulent scales, since an approximation of the Kolmogorov scale in the free shear layers developing away from walls, based on the integral length scale and the turbulent Reynolds number, gives an estimate of $\eta = 29$ µm in fresh gases and more than 200 µm in burned gases. The equivalence ratio of the methane/air flame is around 0.83, corresponding to a thermal flame thickness based on the maximum temperature gradient of about 450 µm. Thus, the progress variable profile is resolved with approximately ten points. Figure 1 shows iso-Q criterion surfaces in the cold flow case to illustrate the high intensity of turbulence that is captured in the DNS, along with an instantaneous temperature field for the reactive case evidencing the high level of wrinkling of the flame front.

3. Flame surface analysis

The DNS database is first used to investigate the estimation of three-dimensional flame surface density Σ from two-dimensional measurements (Σ^{2D}) as obtained, for example, from Rayleigh scattering or planar laser-induced fluorescence, following our work during the last Summer Program (Veynante *et al.* 2010). Two models are compared to DNS data. The first assume isotropic distribution of the instantaneous unit vector normal to the flame front (Σ_{iso}) while the second (Σ_{mod}) involves m_y^{2D}, the fluctuating part of the transverse component of the two-dimensional unit vector normal to the flame front. The measuring plane contains the downstream direction, and the fluctuations of the normal vector are assumed to be similar in both transverse direction, see Veynante *et al.* (2010):

$$\Sigma_{iso} = \frac{4}{\pi}\Sigma^{2D} \quad ; \quad \Sigma_{mod} = \sqrt{\left(1 + \langle m_y^{2D} m_y^{2D} \rangle_s\right)}\,\Sigma^{2D}\,, \tag{3.1}$$

where $< \cdot >_s$ denotes flame surface averages. Figure 2 compares the total flame surface as extracted from DNS and its estimates from Σ_{iso} and Σ_{mod} from two-dimensional "measurements" (also extracted from DNS). Both models perform well even if Σ_{mod} pro-

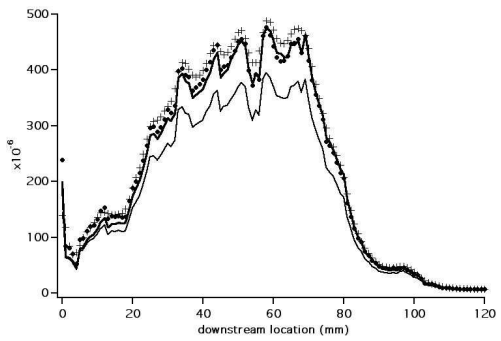

FIGURE 2. Downstream evolution of the total flame surface density $\int\int \Sigma\, dy\, dz$, where y and z denote transverse directions, as extracted from DNS (bold line) and estimated from two-dimensional measurements (Σ^{2D}, thin line) using Eq. (3.1). Dots: Σ_{mod}; crosses: Σ_{iso}.

	Δ_1	Δ_2	Δ_3	Δ_4	Δ_5	Δ_6	Δ_7	Δ_8	Δ_9
Δ [mm]	0.3	0.4	0.6	0.8	1.0	1.2	1.5	2.0	2.5
Δ/h	3.0	4.0	6.0	8.0	10.0	12.0	15.0	20.0	25.0
ℓ_T/Δ	23.0	17.5	11.6	8.7	7.0	5.8	4.6	3.5	2.8
Δ/η	10.0	13.3	20.0	26.6	33.3	40.0	50.0	66.6	83.3
Δ/δ_L	3.8	5.1	7.7	10.2	12.8	15.4	19.2	25.6	32.0
Δ/δ_L^0	0.7	0.9	1.4	1.9	2.3	2.8	3.5	4.7	5.9

TABLE 1. Resolution parameters for the LES filtering. Δ: LES filter size; h: DNS characteristic resolution; ℓ_T: Integral length scale; η: Kolmogorov scale; $\delta_L = \nu/S_L$: Diffusive flame thickness computed from flame speed and molecular viscosity; δ_L^0: thermal flame thickness based on temperature gradient.

vides the best estimate, albeit requiring determination of the instantaneous components of the unit vector normal to the flame front in the measuring plane.

4. A priori test of combustion dynamic modeling

Dynamic modeling of the premixed combustion source is analyzed following the framework proposed by Charlette *et al.* (2002*b*). The generic reaction rate is written as

$$\overline{\dot{\omega}\,(c)} = \Xi_\Delta \frac{W_\Delta\,(\widetilde{c})}{\sqrt{\Delta^2 + {\delta_l^0}^2}}\,, \tag{4.1}$$

while the wrinkling factor, measuring the ratio of SGS to resolved flame surface is given by (Charlette *et al.* 2002*a*):

$$\Xi_\Delta = \left(1 + \min\left[\frac{\Delta}{\delta_L^0} - 1, \Gamma\left(\frac{\Delta}{\delta_L^0}, \frac{u'_\Delta}{S_L^0}, Re_\Delta\right)\frac{u'_\Delta}{S_L^0}\right]\right)^\beta\,, \tag{4.2}$$

where Δ, S_L^0, δ_L^0, u'_Δ, and $Re_\Delta = u'_\Delta\Delta/\nu$ are the filter size, the laminar flame speed and thickness, the SGS turbulence intensity and Reynolds number, respectively, and ν is the fresh gas dynamic viscosity. The reaction rate W_Δ depends only on resolved variables;

here the Boger *et al.* (1998) closure, $W_\Delta = 4\rho_u S_l^0 (6/\pi)\,\widetilde{c}\,(1-\widetilde{c})$, is selected. Charlette *et al.* (2002*b*) suggest looking for a model exponent because a linear expression may lead to an ill-posed problem for large filter size Δ and/or turbulent intensity u'_Δ values, when the resolved contribution to the total flame surface becomes negligible against the unresolved one. The Charlette *et al.* (2002*b*) expressions are slightly modified here. Equation (4.1) was originally derived assuming that $\Delta \gg \delta_L^0$, and the contribution of the laminar flame thickness δ_L^0 was neglected. A (-1) term has also been introduced in Eq. (4.2) to maximize the wrinkling factor to $(\Delta/\delta_L^0)^\beta$ where the model parameter, β, is related to the flame surface fractal dimension D through $\beta = D-2$. As a first step, the wrinkling factor Ξ_Δ is assumed to correspond to this maximum value in the following (i.e., sufficiently large SGS turbulence intensity).

The model parameter β is dynamically determined by writing that the total reaction rate over a given volume, referred as $< \cdot >$, is identical when expressed at scales Δ and $\widehat{\Delta}$ ("Germano-like" identity):

$$\left\langle \left(\frac{\Delta}{\delta_L^0}\right)^\beta \frac{\widehat{W_\Delta\left(\widetilde{c}\right)}}{\sqrt{\Delta^2+{\delta_L^0}^2}} \right\rangle = \left\langle \left(\frac{\widehat{\Delta}}{\delta_L^0}\right)^\beta \frac{W_{\widehat{\Delta}}\left(\widehat{\widetilde{c}}\right)}{\sqrt{\widehat{\Delta}^2+{\delta_L^0}^2}} \right\rangle , \tag{4.3}$$

assuming that the wrinkling factor is constant over the averaging volume, leading to:

$$\beta = \log\left(\frac{\langle \widehat{W_\Delta\left(\widetilde{c}\right)} \rangle \sqrt{\widehat{\Delta}^2+{\delta_L^0}^2}}{\langle W_{\widehat{\Delta}}\left(\widehat{\widetilde{c}}\right)\rangle \sqrt{\Delta^2+{\delta_L^0}^2}} \right) \Bigg/ \log\left(\frac{\widehat{\Delta}}{\Delta}\right) . \tag{4.4}$$

A priori tests of this dynamic model are performed against the DNS database. Volume averaging $< \cdot >$ in Eq. (4.4) corresponds to slices of thickness $\Delta_x = 2.5$ mm in the downstream direction x, and then β depends only on x. Figure 3 (left) displays the downstream evolution of the reaction rate integrated over transverse directions as extracted from the database and estimated from Eqs. (4.1) and (4.4), with $\Xi_\Delta = (\Delta/\delta_L^0)^\beta$ and the Boger *et al.* (1998) model for different values of the LES filter Δ. The resolved contributions, corresponding to $\Xi_\Delta = 1$, are also plotted for reference. Figure 3 (right) displays the spatial evolution of $\beta(x)$.

Mere is good agreement between DNS data and a priori dynamic model predictions. Results also evidence: *i)* the importance of the SGS model as the resolved contribution is far below the total reaction rate (Figure 3 (left)); *ii)* the relevance of a dynamic model as β evolves with x (Figure 3 (right)), showing that a flame/turbulence equilibrium is not reached in the earliest flame developments; *iii)* as expected, β, linked to the flame surface fractal dimension, depends only slightly on the filter size ratio. Overestimation of the modeled reaction at the trailing edge of the turbulent flame ($x \geq 45$ mm, Figure 3) and the corresponding β increase are probably due to the decrease of the turbulent intensity u'_Δ, which are not taken into account here in the wrinkling factor expression Ξ_Δ. This point will be investigated in the future.

5. Subgrid and diffusive fluxes in the $\tilde{c}$ transport equation

In the transport equation for the Favre-filtered progress variable, $\tilde{c}$, the filtered convective flux, $\overline{\rho \mathbf{u} c}$, is usually decomposed as the sum of a resolved flux, $\overline{\rho}\tilde{\mathbf{u}}\tilde{c}$, and an SGS (or turbulent) flux, $\tau_{sgs} = \overline{\rho \mathbf{u} c} - \overline{\rho}\tilde{\mathbf{u}}\tilde{c}$. A gradient diffusion (GD) assumption is often used

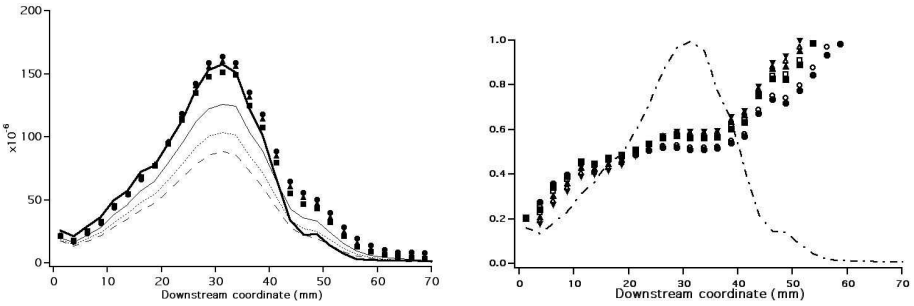

FIGURE 3. Left: Downstream evolution of the reaction rate integrated over transverse directions ($\int\int \overline{\omega}\, dy\, dz$). Bold line: DNS. Markers and thin lines: total and resolved reaction rates ($\widehat{\Delta}/\Delta \approx 2.24$). Square and continuous line: Δ_5; triangle and dotted line: Δ_7; circle and dashed line: Δ_8. Right: Downstream evolution of the $\beta(x)$ model parameter. Circle: Δ_5; square: Δ_7; triangle up: Δ_8; triangle down: Δ_9; filled symbols: $\widehat{\Delta}/\Delta \approx 1.8$; open symbols: $\widehat{\Delta}/\Delta \approx 2.24$. The dotted-dashed line displays the total reaction rate normalized by its maximum values.

to close this subgrid scalar flux:

$$\overline{\rho}\widetilde{u_i c} - \overline{\rho}\tilde{u}_i\tilde{c} = -\frac{\mu_T}{Sc_T}\frac{\partial \tilde{c}}{\partial x_i}\,. \tag{5.1}$$

The turbulent viscosity, μ_T, is estimated with the same model as that appearing in the unclosed SGS stress, and the SGS Schmidt number, Sc_T, is usually fixed to a value smaller than unity. The GD assumption for the subgrid scalar flux has already been challenged in the context of turbulent combustion with RANS (Reynolds Averaging Navier-Stokes), where counter-gradient diffusion has been shown in experiments as well as in DNS (Veynante *et al.* 1997). For LES, previous DNS studies (Domingo *et al.* 2005; Boger *et al.* 1998) have also shown GD and CGD. But contrary to what was observed with RANS, no clear relation with the local intensity of turbulence was found. Moreover, in those DNS, the SGS fluxes were of little consequence compared to the resolved one, suggesting that the error incurred by GD assumption was without much consequence on the LES predictive accuracy. However, these previous DNS were performed with very moderate turbulent Reynolds number (less than 55) and were only two-dimensional. Then, revisiting the SGS scalar flux behavior on the present realistic database with a turbulent Reynolds number of 1,400 will allow those previous observations to be consolidated (or not) and, eventually, will allow construction of a more accurate closure. Figure 4 (top) presents the evolution of the SGS fluxes in the three spatial directions for various filter sizes. Conditional means on the filtered progress variable are used to present the results. As expected, the SGS flux intensity increases as the filter size is increased. The GD assumption (with $Sc_T = 1$) fails to describe the SGS fluxes in x and y directions, which are of CGD type. To avoid spurious error minimization resulting from conditional averaging over all the flame, only a portion of the flow is considered, explaining the different behavior of ∇c in y and z directions in this axisymmetrical flame in mean level. The GD assumption is realistic in the z-direction, with $Sc_T = 0.5$ providing an acceptable agreement, even though the global profile shape is still not fully captured.

Figure 5 presents the divergence of the exact filtered convective scalar flux (continuous line) compared to the divergence of the subgrid scalar flux (continuous line with symbol). Unlike observations on weakly turbulent DNS (Domingo *et al.* 2005), here for representative filter sizes, the subgrid flux contribution is as high as 25% of the total flux in this

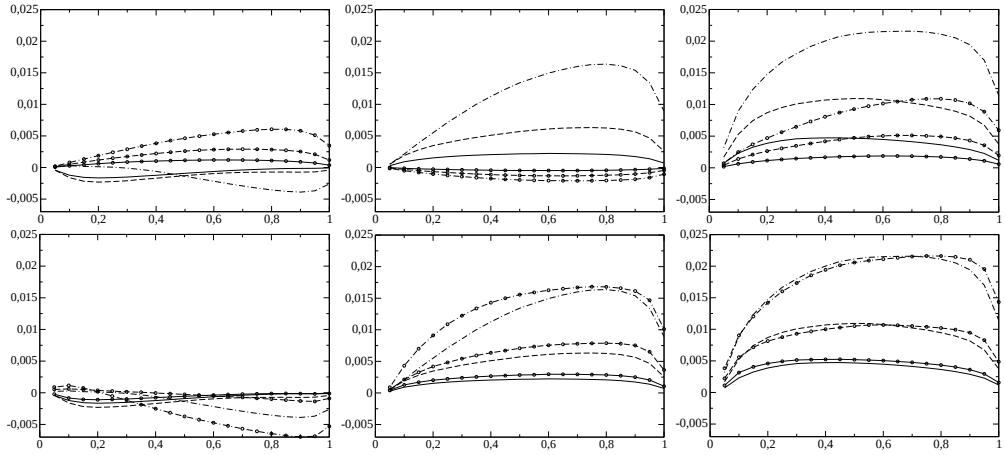

FIGURE 4. SGS turbulent fluxes versus filtered progress variable: x-direction (left), y-direction (center), z-direction (right). DNS (lines) versus model (lines with symbol). Top: gradient closure; bottom: scale similarity hypothesis. Filter sizes: continuous line Δ_1; dashed line: Δ_3; dot-dashed: Δ_6 (see Table 1).

realistic DNS, implying that a reliable closure needs to be provided for the subgrid term. Following the scale similarity approach as originally proposed by Bardina *et al.* (1984), the subgrid scalar flux may be written as

$$\widetilde{u_i c} - \tilde{u}_i \tilde{c} = \mathcal{C} \left(\widehat{\tilde{u}_i \tilde{c}} - \hat{\tilde{u}}_i \hat{\tilde{c}} \right) , \tag{5.2}$$

where $\hat{.}$ represents a filtering operation with a filter test, $\hat{\Delta}$, equal or larger to Δ. The model coefficient $\mathcal{C}$ can either be fixed or determined dynamically as proposed by Salvetti & Banerjee (1995) for the SGS stress tensor. The relation of Eq. 5.2 is compared to the SGS scalar flux extracted from DNS in the Fig. 4 (bottom) with $\mathcal{C} = 1$ and a filter test $\hat{\Delta} = (4/3)\Delta$. In x-direction, the closure performs poorly but the SGS flux is negligible there. Otherwise, the model response stays very close to the exact SGS flux. A dynamic model to determine the parameter $\mathcal{C}$ may help to obtain even better concordance.

Compared to the SGS scalar flux, the filtered diffusive flux appearing in the $\tilde{c}$ transport equation has received less attention in the literature and is usually simply estimated as

$$\overline{\rho \mathcal{D}(T) \frac{\partial c}{\partial x_i}} \sim \overline{\rho} \mathcal{D}(\tilde{T}) \frac{\partial \tilde{c}}{\partial x_i} . \tag{5.3}$$

Recently, Fiorina *et al.* (2010) observed that this simple relation was incorrect even in filtered 1D flames. To quantify the difference between the exact and the resolved diffusive flux, a so-called SGS diffusion flux can be introduced:

$$\tau_{sgs,diff} = \overline{\rho \mathcal{D} \frac{\partial c}{\partial x_i}} - \overline{\rho} \mathcal{D}(\tilde{T}) \frac{\partial \tilde{c}}{\partial x_i} . \tag{5.4}$$

The divergence of this SGS diffusive flux is plotted in Figure 5 (dashed line with symbol). This term is of the same order as the exact term (dashed line) and is as large as the SGS flux due to convection. Then, neglecting it, as is usually done (Eq. 5.3), may lead to an inaccurate estimation of the flame propagation speed. The model proposed by Fiorina *et al.* (2010), which tabulates a correction obtained from a filtered 1D flame, may improve the estimation.

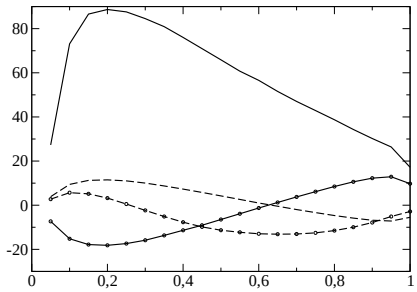

FIGURE 5. Divergence of the convective and diffusive fluxes vs $\widetilde{c}$ for Δ_6. Continuous line: div $(\overline{\rho \mathbf{u} c})$. Continuous line with symbols: div $(\overline{\rho \mathbf{u} c} - \overline{\rho}\tilde{\mathbf{u}}\tilde{c})$. Dashed line: div $\left(\overline{\rho \mathcal{D} \mathbf{grad} c}\right)$. Dashed line with symbols: div $\left(\overline{\rho \mathcal{D} \mathbf{grad} c} - \overline{\rho}\mathcal{D}(\tilde{T})\mathbf{grad}\tilde{c}\right)$.

6. Scalar variance modeling

6.1. *Model description and a priori validation*

The SGS scalar energy is one of the basic inputs of turbulent combustion modeling (Pitsch 2006), for instance to calibrate the shape of presumed probability density functions used to filter tabulated detailed chemistry (Domingo *et al.* 2008). Calculation of the corresponding SGS scalar variances has been the subject of numerous studies and developments (Cook & Riley 1994; Pierce & Moin 1999; Vervisch *et al.* 2010). Approaches based on either direct and dynamic estimations of the variance or on its balance equation have been attempted. An alternative is now discussed, grounded on the exact decomposition of the variance into a part computable from the resolved field and an unknown residual contribution.

Any scalar signal $c(\underline{x},t) = \widetilde{c}(\underline{x},t) + c''(\underline{x},t)$ may be decomposed into $\widetilde{c}(\underline{x},t)$, the filtered part that is resolved on the mesh, and $c''(\underline{x},t)$, an unknown SGS part. Following the so-called modified Leonard decomposition, the SGS variance may be cast in

$$c_v = \widetilde{c c} - \widetilde{c}\,\widetilde{c} = \mathcal{L}_\phi + \mathcal{M}_\phi\,, \tag{6.1}$$

with a resolved term $\mathcal{L}_\phi = \widetilde{\widetilde{c}\,\widetilde{c}} - \widetilde{\widetilde{c}}\,\widetilde{\widetilde{c}}$ and an unknown contribution $\mathcal{M}_\phi = 2(\widetilde{c''\widetilde{c}} - \widetilde{c''}\,\widetilde{\widetilde{c}}) + \widetilde{c''\,c''} - \widetilde{c''}\,\widetilde{c''}$.

In the asymptotic case of a bimodal probability density function of the progress variable c, the SGS variance is a simple function of the resolved function $c_v^{\max} = F_v(\widetilde{c}) = \widetilde{c}(1-\widetilde{c})$. It is proposed to adopt this distribution for the modeled part, but to calibrate its amplitude with a parameter K to be determined dynamically: $\mathcal{M}_\phi = K\,F_v(\widetilde{c})$. The modeled variance would then read

$$c_v = \widetilde{\widetilde{c}\,\widetilde{c}} - \widetilde{\widetilde{c}}\,\widetilde{\widetilde{c}} + K\,F_v(\widetilde{c})\,. \tag{6.2}$$

To compute K dynamically according to local flow properties, a test filtering operation denoted $\hat{\cdot}$ and of size $(4/3)\Delta$ is introduced along with its mass-weighted filtering form $\widetilde{\widetilde{c}}^{\,*} = \widehat{\overline{\rho}\widetilde{c}}/\widehat{\overline{\rho}}$. Both a usual dynamic procedure (Eq. 6.3) and the direct application of the model to the scales between filtered and test filtered (Eq. 6.4) have been attempted to determine K. These two options read as

$$\widetilde{\widetilde{c}\,\widetilde{c}}^{\,*} - \widetilde{\widetilde{c}}^{\,*}\,\widetilde{\widetilde{c}}^{\,*} = \widetilde{\widetilde{\widetilde{c}}\,\widetilde{\widetilde{c}}}^{\,*} - \widetilde{\widetilde{\widetilde{c}}}^{\,*}\,\widetilde{\widetilde{\widetilde{c}}}^{\,*} + K\left[F_v(\widetilde{\widetilde{c}}^{\,*}) - \widetilde{F_v(\widetilde{c})}^{\,*}\right] \tag{6.3}$$

$$= \widetilde{\widetilde{c}}^{\,*}\,\widetilde{\widetilde{c}}^{\,*} - \widetilde{\widetilde{c}}^{\,*}\,\widetilde{\widetilde{c}}^{\,*} + K\,F_v(\widetilde{\widetilde{c}}^{\,*})\,, \tag{6.4}$$

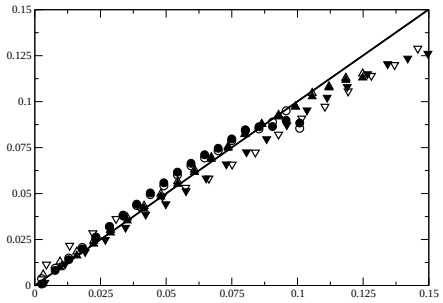

FIGURE 6. A priori test of Eq. (6.2), conditional mean of SGS variance versus DNS. Symbols: Eq. (6.3). Full symbols: Eq. (6.4). Circle: Δ_2; triangle-up: Δ_3; triangle-down: Δ_6 (see Table 1).

in which all terms are computable, to then determine K.

Figure 6 shows the result of *a priori* DNS tests of Eq. (6.2) combined with Eq. (6.4) for the dynamic determination of the parameter K. Here, K is computed at every flow location within the flame, i.e., where $\widetilde{c}$ is different from zero and unity. The conditional mean of the predicted c_v for the values measured in the DNS is shown in Figure 6 for three typical filter sizes. As expected, when the filter size approaches the integral length scale, high levels of SGS variance are difficult to predict (Vervisch *et al.* 2010), but otherwise the model performs well. In the following, Eq. (6.4) is retained to compute K.

6.2. *A posteriori validation*

A priori tests provide a direct assessment of closures in an environment where the relevant variables are known exactly, but those tests obviously suffer from a lack of feedback mechanisms and accumulation of related errors, which must be considered in unsteady simulations (Geurts & Fröhlich 2002). It is therefore essential to proceed with actual LES runs to fully determine the new closure accuracy. To this end, the proposed SGS variance model was implemented in YALES2 during the Summer Program and an LES with a mesh of 14 million tetrahedra ($\Delta/\eta \approx 13$ and $\ell_T/\Delta = 1.77$) was performed using the PCM-FPI closure (Domingo *et al.* 2008), in which the SGS variance calibrates a filtering operation applied to a premixed laminar flamelet with a beta-presumed probability density function.

The mean and rms CO_2 concentration profiles at several locations in the burner are presented in Figure 7. The first conclusion is that Eq. (6.2) couples well with the iterative solution and preserves its prediction capabilities observed in the *a priori* tests; the local SGS variance is then dynamically determined according to local flow properties, without resorting to a balance equation and taking advantage of the exact decomposition of the scalar signal. Notice that this experiment is known to have an important 3/4 wave acoustic mode (Lartigue *et al.* 2004), which could explain an increase of all fluctuation levels which is not fully captured by the present LES.

7. Summary

Estimations of three-dimensional flame surface from two-dimensional measurements have been tested from DNS of a premixed swirl burner. Then, a dynamic formulation

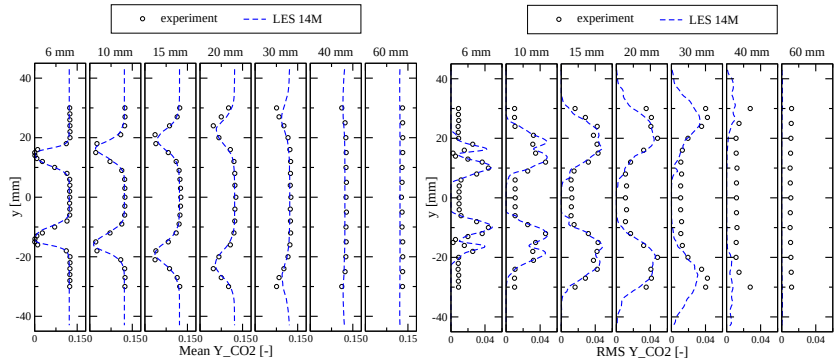

FIGURE 7. CO_2 mass fraction. Left: Mean. Right: Rms. Circle measurement. Dash-line: LES.

for the filtered burning rate of a progress variable has been validated against the DNS results, also used to probe unresolved SGS diffusive and convective fluxes; for the latter, a dynamic formulation was discussed. The unresolved part of the molecular diffusive budget, usually neglected in LES, is found of the same order of magnitude as the transport by unresolved velocity fluctuations. Finally, a new dynamic closure was proposed for the SGS variance of scalar and tested in both *a priori* and full LES of the burner.

Acknowledgments

The authors acknowledge the support of the CTR during the Summer Program and have benefited from fruitful discussions with members of the Combustion Group. This work was granted access to IDRIS HPC resources under the allocation 2010-090052 made by GENCI (Grand Equipement National de Calcul Intensif).

REFERENCES

BARDINA, J., FERZIGER, J. & REYNOLDS, W. 1984 Improved turbulence models based on LES of homogeneous incompressible turbulent flows. *Tech. Rep.* Report TF-19. Stanford University, Thermosciences Division, Dept. Mechanical Engineering.

BOGER, M., VEYNANTE, D., BOUGHANEM, H. & TROUVÉ, A. 1998 Direct numerical simulation analysis of flame surface density concept for large eddy simulation of turbulent premixed combustion. In *Twenty-seventh Symposium (International) on Combustion*, pp. 917–925. The Combustion Institute.

CHARLETTE, F., MENEVEAU, C. & VEYNANTE, D. 2002*a* A power-law flame wrinkling model for LES of premixed turbulent combustion. Part I: Non-dynamic formulation and initial tests. *Combust. Flame* **131** (1/2), 159–180.

CHARLETTE, F., MENEVEAU, C. & VEYNANTE, D. 2002*b* A power-law flame wrinkling model for LES of premixed turbulent combustion. Part II: Dynamic formulation. *Combust. Flame* **131** (1/2), 181–197.

COOK, A. W. & RILEY, J. J. 1994 A subgrid model for equilibrium chemistry in turbulent flows. *Phys. Fluids* **8** (6), 2868–2870.

DOMINGO, P., VERVISCH, L., PAYET, S. & HAUGUEL, R. 2005 DNS of a premixed turbulent V flame and LES of a ducted flame using a FSD-PDF subgrid scale closure with FPI-tabulated chemistry. *Combustion and Flame* **143**, 566–586.

Domingo, P., Vervisch, L. & Veynante, D. 2008 Large-eddy simulation of a lifted methane jet flame in a vitiated coflow. *Combustion and Flame* **152** (3), 415–432.

Fiorina, B., Vicquelin, R., Auzillon, P., Darabiha, N., Gicquel, O. & Veynante, D. 2010 A filtered tabulated chemistry model for LES of premixed combustion. *Combustion and Flame* **157**, 465–475.

Galpin, J., Naudin, A., Vervisch, L., Angelberger, C., Colin, O. & Domingo, P. 2008 Large-eddy simulation of a fuel-lean premixed turbulent swirl-burner. *Combustion and Flame* **155** (1-2), 247–266.

Germano, M., Piomelli, U., Moin, P. & Cabot, W. H. 1991 A dynamic subgrid-scale eddy viscosity model. *Phys. Fluids* **3** (7), 1760–1765.

Geurts, B. J. & Fröhlich, J. 2002 A framework for predicting accuracy limitations in large eddy simulations. *Physics of Fluids* **14** (6), L41–L44.

Hawkes, E. R. & Chen, J. H. 2006 Comparion of direct numerical simulation of lean premixed methane-air flames with strained laminar flame calculations. *Combust. Flame* **144** (1-2), 112–125.

Lartigue, G., Meier, U. & Bérat, C. 2004 Experimental and numerical investigation of self-excited combustion oscillations in a scaled gas turbine combustor. *Applied Thermal Engineering* **24** (11-12), 1583–1592.

Meier, W., Weigand, P., Duan, X. & Giezendanner-Thoben, R. 2007 Detailed characterization of the dynamics of thermoacoustic pulsations in a lean premixed swirl flame. *Combustion and Flame* **150** (1-2), 2–26.

Moureau, V., Domingo, P. & Vervisch, L. 2010 From large-eddy simulation to direct numerical simulation of a lean premixed swirl flame: Filtered laminar flame-pdf modeling. *Submitted*.

Moureau, V., Minot, P., Pitsch, H. & Bérat, C. 2007 A ghost-fluid method for large-eddy simulations of premixed combustion in complex geometries. *Journal of Computational Physics* **221** (2), 600–614.

Pierce, C. & Moin, P. 1999 A dynamic model for subgrid-scale variance and dissipation rate. *Physics of Fluids* **10** (12), 3041–3044.

Pitsch, H. 2006 Large eddy simulation of turbulent combustion. *Annual Review of Fluid Mechanics* **38**, 453–482.

Rivara, M.-C. 1984 Mesh refinement processes based on the generalized bisection of simplices. *SIAM Journal on Numerical Analysis* **21** (3), 604–613.

Roux, S., Lartigue, G., Poinsot, T., Meier, U. & Berat, C. 2005 Studies of mean and unsteady flow in a swirled combustor using experiments, acoustic analysis, and large eddy simulations. *Comb. Flame* **141** (1-2), 40–54.

Salvetti, M. & Banerjee, S. 1995 A priori tests of a new dynamic subgrid-scale model for finite-difference large-eddy simulations. *Physics of Fluids* **7** (11), 2831–2847.

Vervisch, L., Domingo, P., Lodato, G. & Veynante, D. 2010 Scalar energy fluctuations in large eddy simulation of turbulent flames: statistical budget and mesh quality criterion. *Combustion and Flame* **157** (4), 778–789.

Veynante, D., Lodato, G., Domingo, P. & Vervisch, L. 2010 Estimation of three-dimensional flame surface densities from planar images in turbulent premixed combustion. *Experiments in Fluids* **49** (1), 267–278.

Veynante, D., Trouvé, A., Bray, K. N. C. & Mantel, T. 1997 Gradient and counter-gradient scalar transport in turbulent premixed flames. *J. Fluid Mechs* **332**, 263–293.